AMERICAN METEOROLOGICAL SOCIETY

Journal of Hydrometeorology

EARLY ONLINE RELEASE

The DOI for this manuscript is doi: 10.1175/JHM-D-15-0122.1

McEvoy, D., J. Huntington, M. Hobbins, A. Wood, C. Morton, J. Verdin, M. Anderson, and C. Hain, 2016: The Evaporative Demand Drought Index: Part II -- CONUS-wide Assessment Against Common Drought Indicators. J. Hydrometeor. doi:10.1175/JHM-D-15-0122.1, in press.

The Evaporative Demand Drought Index: Part II – CONUS-wide Assessment Against Common Drought Indicators

Daniel J. McEvoy[1, 2], Justin L. Huntington[1, 2], Michael T. Hobbins[3, 4], Andrew Wood[5], Charles Morton[1], James Verdin[6], Martha Anderson[7], and Christopher Hain[8]

[1]Desert Research Institute, Reno, NV

[2]Western Regional Climate Center, Reno, NV

[3]University of Colorado-Cooperative Institute for Research in Environmental Sciences, Boulder, CO

[4]NOAA-Earth Systems Research Laboratory, Physical Sciences Division, Boulder, CO

[5]National Center for Atmospheric Research, Boulder, CO

[6]U.S. Geological Survey Earth Resources Observations and Science Center, Sioux Falls, SD

[7]U.S. Department of Agriculture-Agricultural Research Service, Hydrology and Remote Sensing Laboratory, Beltsville, MD

[8]Earth System Science Interdisciplinary Center, University of Maryland, College Park, MD

Corresponding Author:

Daniel J. McEvoy

Desert Research Institute

Western Regional Climate Center

Reno, Nevada

E-mail: mcevoyd@dri.edu

Abstract

Precipitation, soil moisture, and air temperature are the most commonly used climate variables to monitor drought, however other climatic factors such as solar radiation, wind speed, and humidity can be important drivers in the depletion of soil moisture and evolution and persistence of drought. This work assesses the Evaporative Demand Drought Index (EDDI) at multiple timescales for several hydroclimates as a companion study to Hobbins et al. (2016). We examined EDDI and individual evaporative demand components as they relate to the dynamic evolution of flash drought over the central US, characterization of hydrologic drought over the western US, and comparison to commonly used drought metrics of the US Drought Monitor, Standardized Precipitation Index (SPI), Standardized Soil Moisture Index (SSI), and the Evaporative Stress Index (ESI). Two main advantages of EDDI over other drought indices are that it is independent of precipitation (similar to ESI) and it can be decomposed to identify the role individual evaporative drivers have on drought onset and persistence. At short timescales, spatial distributions and time series results illustrate that EDDI often indicates drought onset well in advance of the USDM, SPI, and SSI. Results illustrate the benefits of physically based evaporative demand estimates, and demonstrate EDDI's utility and effectiveness in an easy-to-implement agricultural early warning and long-term hydrologic drought-monitoring tool with potential applications in seasonal forecasting and fire-weather monitoring.

1. Introduction

Drought is a complex and naturally occurring process with adverse effects on society, primarily through degradation and loss of agricultural crops and depletion of water resources (i.e., streamflow and reservoir storage). Recent examples are instructive: in California, the

extended drought that began in late 2011 is still ongoing, and the 2011-2014 three-year average precipitation (Prcp) record indicates that this period is the second driest in recorded history (Seager et al., 2015); in 2011, Texas experienced extreme Prcp deficits; while in 2011 and 2012 record-breaking temperatures (T_{air}) and high wind speed (U) played a significant role in drought intensification over much of the central US (Karl et al. 2012, Cattiaux and Yiou 2013). Total economic losses are estimated to be $2.7 billion, $7.7 billion, and more than $35 billion for the California, Texas, and central US droughts, respectively. While conditions in Texas deteriorated over many months in 2011, the depletion of moisture over the central US in 2011 occurred at a much faster rate. This fast onset of drought has recently been termed "flash drought" (Svoboda et al. 2002). The physical mechanisms driving flash droughts have been largely neglected from traditional drought metrics. Hence, there is a growing need for continued development of physically based drought metrics that capture Prcp-independent land surface-atmosphere feedbacks; specifically the complementary relationship between actual evapotranspiration (ET) and evaporative demand (E_0).

It has been common practice in recent decades to monitor and analyze drought using metrics driven by Prcp and T_{air} only. The two most commonly used drought indices are the Palmer Drought Severity Index [PDSI; Palmer (1965)], which relies on monthly T_{air} and Prcp, and the Standardized Precipitation Index [SPI; McKee (1993)], which relies on Prcp only. While the PDSI and SPI have proven useful for providing valuable information regarding hydrologic and meteorological drought, these metrics have limitations at short timescales and fail to account for the effects of other important meteorological and radiative forcings such as specific humidity (q), U, and downwelling shortwave radiation (R_d). The most heavily used dataset for decision making with regards to drought is the US Drought Monitor [USDM; Svoboda et al. (2002)],

which relies on a blend of metrics (including PDSI and SPI) and hydrologic data (e.g., soil moisture (SM), streamflow, and snow water equivalent) to produce weekly maps of drought severity. The USDM could be improved through the inclusion of important hydrometeorological forcings key to identifying flash and long-term drought through the use of physically based E_0 estimates.

Other operational products could similarly be improved with the inclusion of physically based E_0 estimates. For example, the US operational PDSI, produced by the National Oceanic and Atmospheric Administration (Heddinghaus and Sabol 1991), continues to use T_{air}-based E_0 estimates (i.e., Thornthwaite 1948) within the PDSI formulation despite the fact that there have been a number of studies that recommend the use of physically based formulations of E_0 (e.g., Palmer 1965; Jensen 1973; Hobbins et al. 2008, 2012; Roderick et al., 2009; Milly and Dunne 2011; Hobbins 2016). Both Dai (2011) and van der Schrier et al. (2011) found PDSI to be largely insensitive to E_0 parameterization during the 20th and early 21st centuries. On the other hand, Sheffield et al. (2012) found major differences between the PDSI driven with T_{air}- and physically based E_0 estimates, especially from the mid-1990s through 2008, with T_{air}-based E_0 estimates showing a significant drying trend, and physically based E_0 estimates indicating no significant trend in global drought severity. The role of physically based E_0 estimates in drought monitoring and prediction remains an active area of research, and is a focus of this paper.

Recent studies have shown that ET, which is obtained through the use of thermal and optical satellite remote sensing or land surface models, used in combination with physically based E_0 can be used as a drought indicator by inherently accounting for feedbacks at the land surface-atmosphere interface through the use of ratios of ET to E_0 (Anderson et al. 2007a, 2007b, 2011; Yao et al. 2010; Mu et al. 2013; Otkin et al. 2013a, 2013b). ET-based drought indices that use

optical and thermal remote sensing, such as the Evaporative Stress Index (ESI; Anderson et al. 2007a, 2007b, 2011), have the advantage of being sensitive to rapid changes in soil moisture conditions that are driven by changes in the atmospheric drivers of T_{air}, U, q, and R_d, and the unique ability to provide early warning of flash drought development (Otkin et al. 2013a). Some of the limitations of using remotely sensed drought indices include cloud cover, satellite inter-arrival times that have to be interpolated, and limited record length for a robust climatology.

To complement indices like ESI, which estimate actual stress on the ground experienced by the vegetation, Hobbins et al. (2016) developed the Evaporative Demand Drought Index (EDDI), a measure of the drying potential of the atmosphere that can presage vegetative stress on the ground. Hobbins et al. (2016) describe two primary physical feedbacks between ET and E_0 that form the rationale for EDDI: a complementary relationship under water-limited conditions (extended drought) where ET and E_0 vary in opposite directions (Bouchet 1963), and a parallel relationship under energy-limited conditions at the onset of flash drought. Under both scenarios, EDDI was found to respond to drying and wetting anomalies of major components of the hydrologic cycle (streamflow, ET, Prcp, and SM) at monthly to annual timescales in several river basins over CONUS with different hydroclimates (Hobbins et al. 2016). At flash drought timescales (weekly to monthly), increased E_0 (high EDDI) may not always lead to vegetative stress. To confirm drought stress, a thermal infrared based remote sensing approach such as ESI can be useful.

This paper builds upon the work of Hobbins et al. (2016) through a CONUS-wide assessment of EDDI against several commonly used drought indices. Data sources and methodology are presented first, followed by comparisons of EDDI to other commonly used drought metrics, flash

114 drought case studies over the central and northeast U.S., and finally, extended drought case
115 studies over the western U.S.

116 **2. Data and Methods**

117 *2.1. Evaporative demand*

118 Various methods have been developed to compute E_0 including T_{air}-based methods (e.g.,
119 Thornthwaite 1948, Hargreaves and Samani 1985), radiation-based methods (Priestley and
120 Taylor 1972), and radiation-aerodynamic combination methods that incorporate maximum
121 temperature (T_{max}), minimum temperature (T_{min}), R_d, *U*, and *q*, such as the Penman-Monteith
122 (PM) approach (Monteith 1965). A priori, it is generally assumed that if the necessary data
123 resources are available, a full-form physically based method, such as PM, should be used over
124 methods based only on T_{air} and/or radiation. Hobbins et al. (2012) and Hobbins (2016)
125 demonstrated that the primary drivers of E_0 variability differ across the US, and with aggregation
126 period (e.g., monthly vs. annual) and season. For example, during summer months *U* is the
127 primary driver of E_0 variability over much of the Great Basin, while R_d is the primary driver of
128 variability over much of the southeast US. In this study, we use reference ET from the PM-based
129 American Society of Civil Engineers Standardized Reference ET equation (ASCE-EWRI, 2005)
130 for E_0. Daily bias-corrected and spatially disaggregated (from 12 km to 4 km) gridded
131 meteorological data [METDATA; Abatzoglou (2011)] are used to compute E_0 on a daily basis
132 for 1979 to 2015. T_{max}, T_{min}, *q* at 2-m, R_d, and *U* [adjusted from 10-m to 2-m following ASCE-
133 EWRI (2005)] were obtained from the University of Idaho
134 (http://metdata.northwestknowledge.net/).

135 *2.2 Evaporative Demand Drought Index*

A probability-based standardized climate variable can be obtained using parametric or non-parametric methods. Parametric methods use a single probability distribution to fit a time series (e.g., Gamma distribution for SPI), where probabilities are transformed to standardized values through an inverse normal approximation. However, a single probability distribution may not always be appropriate at large spatial scales, and several studies have documented these limitations with SPI (Guttman 1999; Quiring 2009) and Standardized Streamflow Index (Vicente-Serrano et al. 2012). The Evaporative Demand Drought Index (EDDI) calculation procedure is presented in Hobbins et al. (2016) and uses a non-parametric probability-based approach to allow for more consistent comparisons between EDDI and other standardized indices.

The EDDI methodology follows Hao and AghaKouchak (2014), where the plotting position approach was used to compute SPI, Standardized Soil Moisture Index (SSI) and Multivariate Standardized Drought Index (MSDI). Farahmand and AghaKouchak (2015) recommend this plotting position approach to maintain consistency when comparing several standardized drought indices.

2.3 Comparison drought metrics

2.3.1 NLDAS-2-based drought indices

To assess the ability of EDDI to identify historical drought periods, EDDI is compared to SPI and SSI using Prcp and simulated SM from NLDAS-2 (Xia et al. 2012a, 2012b). NLDAS-2 Prcp is primarily derived from Climate Prediction Center gridded daily gauge data {with a topographic adjustment from the Parameter-elevation Regressions on Independent Slopes Model [PRISM; Daly et al. (1994)]}. NLDAS-2 SM is derived from the Variable Infiltration Capacity land surface model [VIC; Liang et al. (1994)], and represents the average SM from the top 100

cm of the soil column. Daily NLDAS-2 data were provided (courtesy of Youlong Xia, NCEP) and used only for time series analysis of flash drought case studies (Figure 8). Monthly NLDAS-2 data were obtained for the period of 1979 to 2013 with a native grid spacing of 0.125°. To compare EDDI to NLDAS-2 drought indices, all NLDAS-2 data were resampled to the 4-km (~1/16°) UI METDATA grid using bilinear interpolation. Prcp and SM were accumulated at five timescales (1, 3, 6, 9, and 12 months), and standardized following the EDDI methodology of plotting positions and inverse normal approximation (Hobbins et al. 2016). Pearson linear correlation coefficients between EDDI and standardized NLDAS-2 drought indices were computed for each month (n = 35 years) at the five timescales.

2.3.2 Evaporative Stress Index

The ESI (Anderson et al. 2007b, 2011) represents standardized anomalies in the ET fraction of reference ET (i.e., ET/E_0), with ET obtained through satellite-assisted modeling of the land-surface energy balance. ET and other land-surface energy balance components are retrieved using satellite optical and thermal imagery to force the Atmosphere-Land Exchange Inverse surface energy balance model [ALEXI; Anderson et al. (1997, 2007a)]. Atmospheric variables needed to drive ALEXI come from the North American Regional Reanalysis [NARR; Mesinger et al. (2006)].

Weekly ESI data were provided over the US for 2000 to 2013 at a 4-km spatial resolution and were aggregated to timescales of 1, 2, and 3 months. To obtain a consistent comparison between EDDI and ESI, EDDI was recalculated using the same period of record as the ESI (n = 14 years), and the same aggregation timescales. ESI data were resampled using bilinear interpolation to match the EDDI grid. No downscaling was necessary as both grids were of

identical spatial resolution. Pearson linear correlation coefficients between EDDI and ESI were computed for each week over the 14-year period and at all five timescales.

2.3.3 United States Drought Monitor

The USDM (Svoboda et al. 2002) was used as another metric to assess EDDI, with the primary goal of identifying differences between the two metrics during the evolution of drought through time and space. The USDM is derived from a blend of drought metrics adjusted using local expert knowledge to develop weekly drought severity maps over CONUS (Svoboda et al. 2002; Anderson et al. 2013). The USDM classification system of drought ranges from D0 (abnormally dry) to D4 (exceptional drought). For results where the USDM is compared, all drought metrics were converted to USDM classes (Table 1). The comparisons of EDDI to the USDM are necessarily qualitative because the USDM is a blend of information at several different timescales, whereas EDDI represents a single timescale.

< Table 1 here >

USDM data (2000 to 2013) were downloaded as ESRI shapefiles provided by the National Drought Mitigation Center, and rasterized to match the 4-km EDDI grid, to create a USDM class map of integer values of drought intensity ranging from 0 to 4 (i.e., D0 = 0, D1 = 1, D2 = 2, D3 = 3, and D4 = 4).

3. Results

3.1 NLDAS-2 drought index correlations with EDDI

Temporal correlations between EDDI and NLDAS-2 drought indices (EDDI-SPI and EDDI-SSI) for 1-, 6-, and 12-month timescales are shown in Figure 1. Drought potential and drought itself are indicated by positive EDDI values and negative SPI and SSI values; therefore strong negative correlations represent similar drought signals between EDDI and both SPI and SSI over

204 the 35-year period of record. At the 1 to 12 month timescales correlations between EDDI and
205 SPI and SSI are strongest (more negative) over much of the southwestern and southcentral US
206 (with the exception of 1-month SSI), and highest in Texas (r <-0.7). The northeast is a region of
207 general weak correlations for both EDDI-SPI and EDDI-SSI, with the Midwestern states of OH,
208 IN, and MI being a weak spot for EDDI-SPI only. Spatial correlations at 6- and 12-month
209 timescales are quite similar (Figure 1c-1f), and generally much stronger than at the 1-month
210 timescale (Figure 1a and 1b). Over the northeastern US, EDDI-SPI correlations remain fairly
211 weak at longer timescales, while EDDI-SSI correlations improve over OH, WV, NY, and PA
212 (Figure 1c-1f).

213 Weak correlations to 1-month SSI over the western US may be explained by above-average
214 T_{air} and R_d (driving EDDI upwards) that can lead to increased snowmelt and SM, and a short-
215 term wetting signal from SSI, particularly during the winter months. Positive correlations of
216 EDDI-SPI and EDDI-SSI over the northeastern US are caused by energy-limited conditions, as
217 opposed to water-limited conditions. In such regions, the rate of change in ET is generally
218 proportional and in the same direction as E_0 (Han et al. 2014; Hobbins et al. 2016).

219 **< Figure 1 here >**

220 Figure 2 highlights four regions of interest selected for individual monthly correlation
221 analysis. The Central Valley of California (CA) and Iowa (IA) are two major agricultural regions
222 where drought impacts can have adverse effects on crop production. East-central Texas (TX) is
223 part of a region that has been identified as a global "hot spot" for strong land surface-
224 atmospheric coupling (Koster et al. 2004, 2006); therefore, strong correlation of SM and Prcp to
225 EDDI is expected. Koster et al. (2009) identified Pennsylvania (PA) as an area where generally
226 high SM exerts little control on ET due to prevailing energy-limiting conditions, even during

227 times of severe meteorological drought. This observation is consistent with low correlations
228 found in Figure 1 in parts of the northeast US. The following section further highlights how E_0
229 anomalies (i.e., EDDI) in PA relate to SM- and Prcp-driven droughts.

230 **< Figure 2 here >**

231 Individual monthly correlations between EDDI and NLDAS-2-derived indices at various
232 timescales are shown in Figure 3 for these regions of interest. For each of the selected regions
233 shown in Figure 2, EDDI correlations to SSI and SPI were area-averaged over all pixels. For the
234 TX region (Figure 3a and 3e), seasonality and timescale had little impact on the strength of
235 correlations, and generally showed strong inverse relationships (r < -0.6 for SPI and r < -0.7 for
236 SSI) during most months and timescales, supporting the conclusions of Koster et al. (2004,
237 2006).

238 For the CA region, large seasonal and timescale-dependent variations were found, especially
239 at the 1-month timescale for both SPI and SSI (Figure 3b and 3f). Correlations ranged from
240 +0.20 to -0.82, with the highest correlations occurring at the 6- to 12-month timescales during
241 the growing season. An exceptionally weak correlation (-0.13) was found with SPI during July at
242 the 1-month timescale. July is the driest month of the year for the Central Valley of CA, and
243 most Julys see zero Prcp accumulation. This limits the negative range of the 1-month SPI
244 (McEvoy et al. 2012) causing poor correlations with EDDI. Furthermore, when it does rain
245 during dry summer months it occurs from isolated convective activity over a single day: even if
246 most of the month is warm, cloud-free, and dry (leading to a drought signal from EDDI), the SPI
247 shows a wet anomaly. A more consistent stepped correlation pattern was revealed at longer
248 timescales, where r values < -0.7 were found during the spring (April, May, and June) for 3-

month, spring and summer (July, August, and September) for 6-month, and summer and fall (October, November, and December) for 9- and 12-month periods.

Iowa was similar to TX in that little variability was found in correlations (*r*-values only ranged from -0.5 to -0.7), with the exception of the 1-month timescale. Lower correlations at 1-month timescales during the fall and winter should be expected with SSI, since the top 100 cm of ground is typically frozen during these months, and land surface-atmospheric coupling is weak. There is a rapid increase in correlation at the 1-month timescale during the late spring and summer.

Correlations for the PA region were the weakest of the four analyzed, with notably higher correlations to SSI (Figure 3h) than to SPI (Figure 3d). EDDI is independent of Prcp and can be highly positive even during times of Prcp surplus. However, EDDI is not completely independent of SSI since changes in soil moisture are partially controlled by the drivers of physically based E_0. For SPI (Figure 3d), *r*-values never exceed -0.56, while for SSI (Figure 3h) *r*-values ranged from -0.60 to -0.69 during the summer and early fall at 1-, 3- and 6-month timescales. Weak correlations were found to be both slightly positive and negative ($-0.30 < r < +0.20$) for SPI and SSI at the 1-month timescale during fall and winter, and for winter and spring months at other timescales. Results shown in Figure 3 illustrate that EDDI may be particularly useful for flash drought and seasonal drought monitoring, especially during the growing season.

< Figure 3 here >

3.2 ESI correlations with EDDI

Seasonal temporal correlations between EDDI and ESI for CONUS are shown in Figure 4. Only spring (April, May, and June) and summer (July, August, and September) periods are evaluated due to limited availability of continuous monthly ESI data during fall and winter. ESI

data were frequently missing in snow-covered mountainous regions of the west during spring and summer periods, and ESI pixels were masked (indicated by white shading in Figure 4, as in the mountain ranges of western US) when less than 75% of the monthly time series was available over the period of 2000 to 2013. One benefit of EDDI over ESI and other remote sensing-based metrics is that EDDI can be used during all seasons. This may be particularly useful for high-elevation hydrometeorological monitoring in seasonally snow-covered areas.

Figure 4 illustrates fairly large differences between spring and summer periods, with negligible differences between different timescales of 4-, 8-, and 12-weeks. During the spring period, negative correlations are strongest (r values < -0.7) over much of TX, the desert Southwest, and Central Valley of CA, while weaker relationships were found over the Northeast, and parts of the Pacific Northwest (Figure 4a, 4c, and 4e). The low positive correlations in the Northeast are due to energy-limited evaporative conditions described in Section 3.1. Summer correlations (Figure 4b, 4d, and 4f) are strongest, and spatial patterns most consistent, over the central US, and lower correlations are evident over parts of NV, CA and into the Pacific Northwest when compared to the spring period. Low summer correlations in FL may be due to the shallow water table enhancing actual ET, and EDDI may not be a good indicator of drought potential in this region. Inspection of the summer time series from the regions of low correlation in the West and Pacific Northwest showed that, during certain summers, ESI and EDDI were strongly negatively correlated but positively correlated in others (not shown). ET rates in semi-arid regions are typically low during summer periods; therefore small variations in ET can potentially lead to large changes in ESI, making for poor correlations with EDDI. For example, most of NV experienced below normal Prcp and high temperatures for July of 2005, and EDDI and SPI indicated drought conditions, whereas ESI indicated wet conditions (not shown). In

295 general, EDDI is strongly correlated to ESI (r values < -0.7) during spring and summer months
296 over much of the Southwest, south-central, and north-central US.

297 **< Figure 4 here >**

298 *3.3 Flash drought during the growing season*

299 Flash drought can develop even during periods of normal or excess Prcp, and evaporative
300 drivers can uniquely identify the onset and evolution of flash drought. For example, in some
301 situations, a T-based E_0 would fail to identify rapid drying due to below-normal T_{air} coincident
302 with high U and low q. The following highlights the Midwest droughts of 2011 and 2012 and
303 several other case studies in the central and northeastern US to demonstrate how EDDI can serve
304 as an effective early warning of flash droughts.

305 Area-averaged time series of 1-month EDDI are compared to 1-month SPI and SSI during
306 2011 and 2012 in Figure 5 for the IA domain. Note that the vertical axis of EDDI is inverted to
307 better visualize drought onset and duration when compared to SPI and SSI in Figure 5.

308 Figure 5 illustrates that in April of 2011, all indices are near neutral (i.e., close to zero), and
309 over the next two months EDDI changes to a moderate drought class (> 0.78 or USDM D1
310 class), while both SPI and SSI increase to slightly wet conditions. SPI and SSI values show no
311 decrease until July of 2011 (see black box in Figure 5). EDDI reaches D1 in June, while SSI and
312 SPI reach D1 in September indicating a 3-month lead provided by EDDI. SPI falls below
313 moderate drought in September, and SSI follows one month later in October. Both EDDI and
314 SSI maintain extended drought conditions throughout all of 2012, with the exception of February
315 when EDDI is slightly above moderate drought (0.78), but still below zero. During this extended
316 drought of 2012, SPI is highly variable and indicates wet conditions for many months.

317 **< Figure 5 here >**

To highlight the E_0 drivers that caused EDDI to signal first a flash drought and then an extended drought, a simple sensitivity analysis of EDDI was performed (Figure 6a and 6b). For this analysis, E_0 was calculated while constraining the variable of interest to daily climatology values in order to isolate the impact of each forcing on the EDDI drought signal. Results are presented as estimates of EDDI with a notation of the variable of interest (i.e., EDDI-T, EDDI-q, EDDI-R_d, and EDDI-*U*). For example, EDDI-T was calculated using the daily climatology of T_{max} and T_{min}, and with METDATA-observed values for all other variables. During the period of 20-25 May, 2011, EDDI-q and EDDI-*U* had the greatest separation from standard EDDI values in the negative direction (note y-axis is inverted), which indicates that the drying power of the air term in the E_0 equation (*U* multiplied by vapor pressure deficit), initiated the flash drought signal in EDDI via increased *U* and below normal *q* (Figure 6b) during the period 20 May through 5 June. In this case, using daily climatology *q* and *U* values mitigated the drought signal relative to the standard EDDI. By June, 2011, EDDI decreased below the moderate drought threshold (0.78), with the primary difference from May being that *U* and T_{air} were then acting in combination to exacerbate the drought signal—as opposed to T_{air} moderating it in May. Despite below-normal T_{air} conditions in September, 2011 (Figure 6a), the standard EDDI drought signal was maintained due to extremely low *q* values evidenced by a large difference between EDDI and EDDI-q (absolute difference of 1.17). From November, 2011 through May, 2012, T_{air} dominated the EDDI signal, as seen by the large differences between EDDI and EDDI-T. This increase in T_{air} and E_0 likely contributed to the persistent SSI drought signal throughout 2012, despite above-normal Prcp for February, April, October, and December (see Figure 5).

< Figure 6 here >

To spatially assess EDDI during the 2012 drought, a comparison was made between the USDM, SPI, SSI, and ESI. Recall from Section 2.5 that the USDM is a blend of products at various time-scales, but we are comparing it here to a fixed time-scale EDDI: thus, the EDDI and the USDM distributions should not be expected to be identical. The objective of the EDDI and USDM comparisons is to show that EDDI can presage rapid onset droughts before the impacts show up in the USDM, thus highlighting the substantial added value gained by using EDDI in conjunction with other drought-monitoring metrics for decision-making applications.

Figure 7 shows the evolution of the 1-month EDDI, ESI, SSI, and SPI, and USDM through time and space over the spring and summer of 2012. The USDM generally indicated no drought or only D1-D2 over much of the central US as of 1 May (Figure 7, row 1, column 1). In contrast, EDDI indicates at least moderate drought conditions over most of the same region, and looks similar to the USDM spatial distribution of two months later (i.e., of 3 July, 2012). EDDI responded to anomalously high T_{air}, U, and R_d across the region during the second half of April. ESI showed widespread neutral conditions for April with a rapid intensification in May. SSI and SPI show a slower progression and more local intensification (non-uniform spatial distribution) when compared to EDDI and ESI. The 2012 drought evolution illustrated by the USDM over the central US expands in both spatial extent and severity throughout the summer, however the progression from D0 to D3 and D4 takes approximately three months. Figure 7 illustrates that 1-month EDDI presaged the onset of USDM extreme to exceptional drought (D3-D4) by as much as two months. This case study highlights the application of using EDDI to identify future drought potential and onset of drought.

< Figure 7 here >

Four additional flash drought cases from PA, NY, WI, and the OH-IN border are presented in Figure 8 using daily time series of 1-month EDDI, SPI, and SSI during the growing season (April through September). Two of these cases (WI 2002 and OH-IN 2007) are examples from Otkin et al. (2013b). Two new cases (PA 1983 and NY 1991) are presented in this study to show that EDDI is effective in energy-limited regions such as PA, despite low correlations to SPI there (see Figure 3d). All four case studies are located in major agricultural regions. Domains used for spatial averaging are presented in Figure 2. For the PA case, EDDI decays rapidly from neutral to severe drought in ten days starting around day 180. At the same time, there is a rapid spike in SPI to moderate wetness and then a slow decline towards drought and another rapid decline from days 206 to 210. Both EDDI and SPI converge on extreme drought at day 210, while the slower-to-respond SSI never reaches the extreme drought criterion. This type of signal, where EDDI shows a rapid change and SPI and SSI slowly move towards drought, could be used as a warning signal for potential on-the-ground drought impacts. For the NY case, both EDDI and SPI show two distinct rapid declines, the first at day 140 and the second at days 156 (SPI) and 157 (EDDI), with EDDI reaching drought threshold prior to SPI. The EDDI drought peaks about day 160, SPI at 180, and SSI around 220. For WI, EDDI and SPI are closely correlated during the onset of drought, but SPI maintains a longer and more severe drought. The OH-IN case is similar to the PA case in that EDDI shows the flash drought (starting at day 128) well in advance of the crash of SPI that starts at day 145. In all four cases, EDDI is able to detect the flash drought prior to, or at the same time as, SPI and always ahead of the SSI signal.

< Figure 8 here >

Results illustrated in Figures 5-8 of this paper and in the companion paper (Hobbins et al. 2016) highlight two major focal points of this research: (1) EDDI is a leading indicator of flash

drought conditions; and (2) a physically based E_0 is required to capture this signal. This reinforces the work of Hobbins et al. (2012) and Hobbins (2016), who concluded that T_{air} is not always the dominant driver of E_0, and that T-based parameterizations could lead to false drying (or wetting) signals when used for drought-monitoring applications. Our findings (illustrated in Figure 5) also contradict the notion that 2012 should be considered a flash drought case over the central IA (in contrast to Mo and Lettenmaier 2015): our results clearly indicate a well-established and persistent drought signal by both EDDI and SSI, with SPI being the only indicator to signal a rapid transition from wet to dry over the period of April through July. Figure 5 illustrates that the flash drought signal appeared in EDDI starting in May, 2011, and in SPI and SSI starting in August, 2011.

3.4 Extended drought in arid to semi-arid regions

In this section we examine whether EDDI can be used to characterize historical extended droughts over the western US. Droughts in arid to semi-arid regions of the US are generally slower to develop than in the central US, primarily due to the manner in which water resources are both naturally and anthropogenically stored. Natural water storage occurs as winter snowpack at high elevations that typically reach maximum depth in March or April. During spring and summer snowmelt, runoff is stored in reservoirs. Hydrologic drought severity in the West is strongly linked to reservoir storage and streamflow (McEvoy et al. 2012, Abatzoglou et al. 2014).

Four extended drought case studies using the USDM, EDDI, SPI, and SSI are shown in Figure 9. The first case focuses on the extreme southwestern drought of 2002 (Figure 9, first column), with the USDM mapped at 25 June, 2002 (Figure 9a), and the 6-month EDDI, SPI, and SSI mapped for January through June, 2002 (Figure 9e, 9i, and 9m, respectively). All metrics

show a similar spatial structure of drought extent, although EDDI and SPI indicate little to no drought in MT. Temperatures were lower than normal over much of MT, WY, and the northern portions of UT and CO, and slightly above normal for the Four Corners region (not shown). This indicates that T_{air} was likely driving EDDI negative in MT; however T_{air}, q and U must have all played a role in driving EDDI in the positive direction over UT and CO.

The second case focuses on the drought of the 2007 water year (October, 2006, through September, 2007; Figure 9, second column). The USDM from 02 October, 2007, indicates 78% (percent area) of the western US in at least D0 (Figure 9b). Figure 9f illustrates the 12-month EDDI ending in September, 2007, and has the strongest spatial coherence and severity when compared to the USDM, while SSI and SPI (Figure 9j and 9n, respectively) underrepresent the spatial extent shown by USDM and EDDI, particularly over NV, ID, and western MT.

The third case highlights the extraordinary snow drought that occurred during the winter of 2014-2015 (Figure 9, third column). At the end of March, 2015, the USDM continued to show D3 and D4 over much CA and NV, but little to no drought over the WA Cascades and northern Rockies of ID and MT (Figure 9c). The October, 2014, through March, 2015, period saw near-normal or even slightly above normal Prcp over much of the Pacific NW, which is reflected in the 6-month SSI (Figure 9k) and SPI (Figure 9o). However, record warmth during this period led to extremely freezing levels and much of the Cascade Range measured snowpacks of less than 25% of normal by the end of March (not shown). Record warmth and lack of Prcp led to similar snowpack conditions over the Sierra Nevada. The 6-month EDDI is the only indicator to reflect the snow drought conditions in the Cascades and northern Rockies (Figure 9g). Case four (Figure 9, fourth column) shows that by the end of August, 2015, the USDM showed WA 100% covered by D2 (13.36%) and D3 (86.64%) with widespread D3 over northern ID and western MT (Figure

9d). Six-month EDDI (Figure 9h), SSI (Figure 9l), and SPI (Figure 9p) all agree at this point and show widespread D3 and D4 over the Cascades, northern ID and MT. Summer of 2015 was a devastating wildfire season for CA and much of the Pacific Northwest with close to 10 million acres burned in the US (National Interagency Fire Center; https://www.nifc.gov/fireInfo/fireInfo_stats_totalFires.html), a result of the snow drought and record winter warmth followed by a hot and dry summer. Cases three and four (Figures 9g and 9h) demonstrate that EDDI is not only a drought indicator, but can also potentially serve as a wildfire risk indicator. Further research on relationships between EDDI and wildfire risk will be conducted in future studies.

< Figure 9 here >

The potential usefulness of EDDI to aid in the interpretation of hydroclimatic states at multiple timescales and over long time periods is assessed in Figure 10, which illustrates time series of EDDI averaged over the northern Sierra Nevada for 1979-2014. As the northern Sierra Nevada provides much of the water resources to western NV and CA, the use of multiple complementary drought metrics for evaluating short and extended drought in this region is invaluable. EDDI at the 2-week and 1-month timescales (Figure 10a and 10b, respectively) closely correspond to documented heat waves and extreme fire weather in the region (Burt 2007; Trouet et al. 2009). However the high frequency of the time series (Figure 10a and 10b) make it difficult to characterize hydrologic drought. At longer timescales (Figure 10c, 10d, and 10e, respectively) EDDI clearly identifies all of the major documented hydrologic droughts over the period from 1979 to 2014 (Seager 2007; Weiss et al. 2009; McEvoy et al. 2012). The ongoing drought that began in late 2011 clearly stands out as most severe and longest-duration event of the analyzed period. Fast recovery of hydrologic droughts are also well captured by EDDI at

nearly all timescales when compared to known "drought-buster" Prcp events (Ralph and Dettinger 2010; Dettinger 2013), and wet periods associated with El Niño (1982-83 and 1997-98), and La Niña (2010-11).

< Figure 10 here >

4. Discussion

Correlations of EDDI to NLDAS-2-forced drought metrics of SSI and SPI indicate that over much of CONUS, EDDI spatial distributions are generally similar to SPI and SSI. However, over parts of CONUS weak correlations were found. Comparisons of EDDI to remotely sensed ESI products also show strong correlations over much of CONUS, with the exceptions of the northeast US during spring, and over parts of the western US during summer. One reason for weak correlations with ESI over the northeastern US are largely due to energy-limited land-surface energy-balance conditions over the region, where ET and E_0 are often positively correlated. The two main reasons why EDDI showed weak correlations to other drought metrics are that (1) EDDI often is a leading indicator and so there is a lag present in the time series and (2) EDDI can be strongly positive even when moisture deficits are not present on the ground, but are rapidly being depleted due to high evaporative demand. It can be difficult to distinguish between these two signals in EDDI at short timescales: drought early warning vs. false alarm; however a false alarm would only occur if soil moisture was replenished via an intense precipitation event. Our analysis highlights the advantage of using EDDI to monitor potential and actual drought development. When EDDI is used in combination with ESI, actual drought stress may be better understood. A key strength of EDDI is that it can be effectively used to provide year-round data, with no limitations during cloudy days or over snow-covered areas.

For drought monitoring in arid and semi-arid regions of the western US, EDDI aggregation to longer timescales (3 to 12 months) is best suited to capture the complementary relationship found between ET and E_0 (Bouchet 1963; Hobbins et al. 2004), and therefore identify and monitor extended hydrologic droughts typical of this region. Results illustrate that in most cases, when Prcp deficits at the 3- to 12-month timescales were fairly large, EDDI was strongly positive. The primary limitation of EDDI for hydrologic drought monitoring is that during cold droughts EDDI may not be able to capture severity due to the sensitivity to T_{air}.

5. Summary and conclusions

This work highlights an application and assessment of EDDI at multiple timescales and for several hydroclimates as a companion study to Hobbins et al. (2016). The methods and results of Hobbins et al. (2016) are reinforced and a CONUS-wide evaluation is performed, by examining EDDI and individual evaporative demand components as they relate to the dynamic evolution of flash drought over the central US, characterization of hydrologic drought over the western US, and comparison to commonly used drought metrics (USDM, SPI, SSI, and ESI). The major findings from this work are summarized as follows:

- EDDI was able to identify droughts over CONUS consistent with SPI, SSI, and ESI.
- For flash drought monitoring, EDDI showed potential development and onset of drought up to two months in advance of the USDM and often led SPI and SSI.
- A unique advantage of EDDI is the ability to decompose droughts and test the sensitivity of EDDI to E_0 drivers. High U and low q played a major role in initiating the 2011 flash drought case in IA. This was followed by extreme positive T_{air} anomalies that drove much of the EDDI drought signal in 2012 and exacerbated the depletion of SM.

- Tracking drought using sub-monthly data and multiple drought indices (Figure 8) can add value to operational drought monitoring relative to simply using monthly data. Flash droughts are dynamic, with large changes in moisture availability possible over a 1-month period, even when considering a time series run through a 30-day smoothing filter (i.e., a 1-month drought index timescale).
- Despite being independent of precipitation, EDDI is able to capture long-term hydrologic and snow drought in the western US.

Despite some limitations, EDDI is shown to provide useful information on the less-understood and documented dynamical processes associated with drought evolution and persistence. Results highlighted in this work illustrate the benefits of assimilating physically based E_0 estimates and EDDI into operational monitoring products such as the USDM. The additional information and early warning provided by EDDI could greatly contribute to a stronger understanding of drought evolution and dynamics, land surface-atmosphere interactions, and, perhaps more importantly, reduce and/or mitigate future adverse societal effects that have been associated with past droughts. EDDI could also prove useful and effective for easy-to-implement operational early warning for agricultural and fire-weather monitoring (Ham et al. 2014) and seasonal forecasting of drought (McEvoy et al., 2016).

Acknowledgments

Authors Dr. McEvoy, Dr. Huntington, and Mr. Morton were supported by the Desert Research Institute (DRI) Maki Endowment for enhancing water resource monitoring in Southern Nevada grant #6223-640-0969, U.S. Bureau of Reclamation Climate Analysis Tools WaterSMART program grant # R11AP81454, and a U.S. Geological Survey and DRI Great Basin Cooperative Ecosystem Study Unit collaborative project on drought monitoring and fallow

field-tracking through cloud computing of Landsat, MODIS, and gridded climate data archives grant #G15AC00137.

References

Abatzoglou, J.T., 2011: Development of gridded surface meteorological data for ecological applications and modelling. *Int. J. Climatol*. **33**, 121–131, doi:10.1002/joc.3413.

Abatzoglou, J.T., R. Barbero, J. Wolf, and Z. Holden, 2014: Tracking interannual streamflow variability with drought indices in the U.S. Pacific Northwest. *J. Hydrometeor*. **15**, 1900–1912, doi:10.1175/JHM-D-13-0167.1.

Anderson, M.C., J.M. Norman, G.R. Diak, W.P. Kustas, and J.R. Mecikalski, 1997: A two-source time-integrated model for estimating surface fluxes using thermal infrared remote sensing. *Remote Sens. Environ.*, **60**, 195–216. doi:10.1016/S0034-4257(96)00215-5.

Anderson, M.C., J. M. Norman, J.R. Mecikalski, J.A. Otkin, and W.P. Kustas, 2007a: A climatological study of evapotranspiration and moisture stress across the continental United States based on thermal remote sensing: 1. Model formulation, *J. Geophys. Res.*, **112**, D10117, doi:10.1029/2006JD007506.

Anderson, M.C., J.M. Norman, J.R. Mecikalski, J.A. Otkin, and W.P. Kustas, 2007b: A climatological study of evapotranspiration and moisture stress across the continental United States based on thermal remote sensing: 2. Surface moisture climatology, *J. Geophys. Res.*, **112**, D11112, doi:10.1029/2006JD007507.

Anderson, M.C., C. Hain, B. Wardlow, A. Pimstein, J.R. Mecikalski, and W.P. Kustas, 2011: Evaluation of drought indices based on thermal remote sensing of evapotranspiration over the continental United States. *J. Climate*, **24(8)**, 2025–2044, doi:10.1175/2010JCLI3812.1.

544 Anderson, M.C., C. Hain, J. Otkin, X. Zhan, K. Mo, M. Svoboda, B. Wardlow, and A. Pimstein,
545 2013: An intercomparison of drought indicators based on thermal remote sensing and
546 NLDAS-2 simulations with U.S. Drought Monitor classifications. *J. Hydrometeor.*, **14**,
547 1035–1056, doi:10.1175/JHM-D-12-0140.1.
548 ASCE-EWRI, 2005: The ASCE Standardized Reference Evapotranspiration Equation. Report 0-
549 7844-0805-X, 59 pp. [Available online at
550 http://www.kimberly.uidaho.edu/water/asceewri/ascestzdetmain2005.pdf.]
551 Bouchet, R.J., 1963: Évapotranspiration réelle et potentielle, signification climatique. *Proc.*
552 *International Association Scientific Hydrology Symp., Publ. No. 62*, Berkeley, CA,
553 International Association Scientific Hydrology, 134–142.
554 Burt, C.C., 2007: *Extreme weather: a guide and record book*. W.W. Norton and Co., 320 pp.
555 Cattiaux, J., and P. Yiou, 2013: U.S. heat waves of spring and summer 2012 from the flow-
556 analogue perspective [in "Explaining Extreme Events of 2012 from a Climate Perspective"].
557 *Bull. Amer. Meteor. Soc*., **94(9)**, S10–S13. doi: http://dx.doi.org/10.1175/BAMS-D-13-
558 00085.1.
559 Dai, A., 2011: Characteristics and trends in various forms of the Palmer Drought Severity Index
560 during 1900-2008, *J. Geophys. Res*., **116**, D12115, doi:10.1029/2010JD015541.
561 Daly, C., R.P. Neilson, and D.L. Phillips, 1994: A statistical-topographic model for mapping
562 climatological precipitation over mountainous terrain. *J. Appl. Meteorol.*, **33(2)**, 140–158.
563 doi: http://dx.doi.org/10.1175/1520-0450(1994)033<0140:ASTMFM>2.0.CO;2.
564 Dettinger, M.D., 2013. Atmospheric rivers as drought busters on the U.S. West Coast. *J.*
565 *Hydrometeor*., **14(6)**, 1721–1732, doi: 10.1175/JHM-D-13-02.1.

566 Farahmand, A., and A. AghaKouchak, 2015: A generalized framework for deriving
567 nonparametric standardized indicators. *Adv. Water Resour.*, **76**, 140–145,
568 doi:10.1016/j.advwatres.2014.11.012
569 Guttman, N.B., 1999: Accepting the standardized precipitation index: a calculation algorithm. *J.*
570 *Amer. Water Resour. Assoc.* **35(2)**, 311–322. doi: 10.1111/j.1752-1688.1999.tb03592.x.
571 Ham, C., M.T. Hobbins, K.L. Abt, and J.P. Prestemon, 2014: Using the Evaporative Demand
572 Drought Index and the Palmer Drought Severity Index to forecast the number of large
573 wildland fires on federal lands, *Large Wildland Fires Conference*, Missoula, MT,
574 Association for Fire Ecology and the International Association of Wildland Fire. [Available
575 online at http://largefireconference.org/wp-content/uploads/2013/06/Oral-Presentation-
576 Abstracts-V4.pdf.]
577 Han, S., F. Tian, and H. Hu, 2014: Positive or negative correlation between actual and potential
578 evaporation? Evaluating using a nonlinear complementary relationship model. *Water*
579 *Resources Research*, 50(2), 1322–1336. doi: 10.1002/2013WR014151.
580 Hao, Z., and A. AghaKouchak, 2014: A nonparametric multivariate multi-index drought
581 monitoring framework, *J. Hydrometeor.*, **15**, 89–101, doi:10.1175/JHM-D-12-0160.1.
582 Hargreaves, G.H., and Z.A. Samani, 1985: Reference crop evapotranspiration from temperature,
583 *Appl. Eng. Agric*., **1**, 96–99. doi: 10.13031/2013.26773.
584 Heddinghaus, T.R., and P. Sabol, 1991: A review of the Palmer Drought Severity Index and
585 where do we go from here? *Preprints, Seventh Conf. on Applied Climatol*ogy, Boston, MA,
586 Amer. Meteor. Soc., 242–246. [Available online at http://www.ncdc.noaa.gov/temp-and-
587 precip/drought/docs/heddinghaus-sabol-pmdi-article.pdf.]

588 Hobbins, M.T., J.A. Ramírez, and T.C. Brown, 2004: Trends in pan evaporation and actual
589 evaporation across the conterminous U.S.: Paradoxical or complementary? *Geophys. Res.*
590 *Lett.*, **31(13)**, L13503, doi: 10.1029/2004GL0198426.
591 Hobbins, M.T., A. Dai, M.L. Roderick, and G.D. Farquhar, 2008: Revisiting the
592 parameterization of potential evaporation as a driver of long-term water balance trends.
593 *Geophys. Res. Lett.*, **35**, L12403, doi: 10.1029/2008GL033840.
594 Hobbins, M.T., A.W. Wood, D. Streubel, and K. Werner, 2012: What drives the variability of
595 evaporative demand across the conterminous United States? *J. Hydrometeor.*, **13**, 1195–
596 1214, doi: 10.1175/JHM-D-11-0101.1.
597 Hobbins, M.T., A. Wood, D.J. McEvoy, J.L. Huntington, C. Morton, and J. Verdin, 2016: The
598 Evaporative Demand Drought Index: Part I - linking drought evolution to variations in
599 evaporative demand. *J. Hydrometeor.* (this issue).
600 Hobbins, M.T., 2016: The variability of ASCE Standardized Reference Evapotranspiration: a
601 rigorous, CONUS-wide decomposition and attribution. *Trans. ASABE*, 59(2), doi:
602 10.13031/trans.5910975, in press.
603 Jensen, M. E., 1973: *Consumptive use of water and irrigation water requirements*. New York,
604 NY: American Society of Civil Engineers.
605 Karl T.R., and Coauthors, 2012: U.S. temperature and drought: recent anomalies and trends. *Eos*
606 *Trans. AGU*, **93(47)**, 473–474. doi:10.1029/2012EO470001.
607 Koster, R.D., and Coauthors, 2004: Regions of strong coupling between soil moisture and
608 precipitation. *Science*, **305(5687)**, 1138–1140, doi: 10.1126/science.1100217.
609 Koster, R.D., and Coauthors, 2006: GLACE: The Global Land–Atmosphere Coupling
610 Experiment. Part I: Overview. *J. Hydrometeor*., **7**, 590–610, doi:10.1175/JHM510.1.

611 Koster, R.D., S.D. Schubert, and M.J. Suarez, 2009: Analyzing the concurrence of
612 meteorological droughts and warm periods, with implications for the determination of
613 evaporative regime. *J. Climate*, **22**, 3331–3341, doi: 10.1175/2008JCLI2718.1.
614 Liang, X., D.P. Lettenmaier, E.F. Wood, and S.J. Burges, 1994: A simple hydrologically based
615 model of land surface water and energy fluxes for general circulation models. *J. Geophys.*
616 *Res.*, **99(D7)**, 14,415–14,428. doi: 10.1029/94JD00483.
617 Mesinger, F., and Coauthors, 2006: North American Regional Reanalysis. *Bull. Amer. Meteor*.
618 *Soc*., **87(3)**, 343–360, 10.1175/BAMS-87-3-343
619 McEvoy, D.J., J.L. Huntington, J.T. Abatzoglou, and L.M. Edwards, 2012: An evaluation of
620 multiscalar drought indices in Nevada and eastern California. *Earth Interact*., **16**, 1–18,
621 doi:10.1175/2012EI000447.1.
622 McEvoy, D.J., J.L. Huntington, J.F. Mejia, and M.T. Hobbins, 2016: Improved seasonal drought
623 forecasts using reference evapotranspiration anomalies. *Geophys. Res. Lett.*, **43**, 377-385,
624 doi: 10.1002/2015GL067009.
625 McKee, T.B., N.J. Doesken, and J. Kleist, 1993: The relationship of drought frequency and
626 duration to time scales. *Preprints, Eighth Conf. on Applied Climatology*, Anaheim, CA,
627 Amer. Meteor. Soc., 179–184. [Available online at
628 http://ccc.atmos.colostate.edu/relationshipofdroughtfrequency.pdf.]
629 Milly, P.C.D., and K.A. Dunne, 2011: On the hydrologic adjustment of climate-model
630 projections: the potential pitfall of potential evapotranspiration. *Earth Interact.*, **15**,
631 doi:10.1175/2010EI363.1.
632 Mo, K.C., and D.P. Lettenmaier, 2015: Heat wave flash droughts in decline. *Geophys. Res. Lett.*,
633 **42**, 2823–2829, doi:10.1002/2015GL064018.

634 Monteith, J.L., 1965: Evaporation and environment. *Symp. Soc. Exp. Biol.*, **XIX**, 205–234.
635 Mu, Q., M. Zhao, J.S. Kimball, N.G. McDowell, and S.W. Running, 2013: A remotely sensed
636 global terrestrial drought severity index. *Bull. Amer. Meteor. Soc.*, **94(1)**, 83–98,
637 doi:10.1175/BAMS-D-11-00213.1.
638 Otkin, J.A., M.C. Anderson, C. Hain, I.E. Mladenova, J.B. Basara, M. Svoboda, 2013a:
639 Examining rapid onset drought development using the thermal infrared–based Evaporative
640 Stress Index. *J. Hydrometeor.*, **14**, 1057–1074. doi:10.1175/JHM-D-12-0144.1.
641 Otkin, J.A., M.C. Anderson, C. Hain, and M. Svoboda, 2013b: Examining the relationship
642 between drought development and rapid changes in the Evaporative Stress Index. *J.*
643 *Hydrometeor.*, **15**, 938–956, doi:10.1175/JHM-D-13-0110.1.
644 Palmer, W.C., 1965: Meteorological drought. Research Paper 45, 58 pp. [Available online at
645 http://www.ncdc.noaa.gov/temp-and-precip/drought/docs/palmer.pdf.]
646 Priestley, C.H.B., and R.J. Taylor, 1972: On the assessment of surface heat flux and evaporation
647 using large-scale parameters. *Mon. Weather Rev*., **100(2)**, 81–92. doi:
648 http://dx.doi.org/10.1175/1520-0493(1972)100<0081:OTAOSH>2.3.CO;2.
649 Quiring, S.M., 2009: Developing objective operational definitions for monitoring drought. *J.*
650 *Appl. Meteor. Climatol.* **48**, 1217–1229, doi: 10.1175/2009JAMC2088.1.
651 Ralph, F.M., and M.D. Dettinger, 2012: Historical and national perspectives on extreme West
652 Coast precipitation associated with atmospheric rivers during December 2010. *Bull. Amer.*
653 *Meteor. Soc.*, **93**, 783–790. doi:10.1175/BAMS-D-11-00188.1.
654 Roderick, M. L., M. T. Hobbins, and G. D. Farquhar, 2009: Pan evaporation trends and the
655 terrestrial water balance II. Energy balance and interpretation, *Geography Compass*, 3, 761-
656 780, doi: 10.1111/j.1749-8198.2008.00214.x.

Seager, R., 2007: The turn of the century North American drought: global context, dynamics, and past analogs. *J. Climate*, **20**, 5527–5552, doi:10.1175/2007JCLI1529.1.

Seager, R., M. Hoerling, S. Schubert, H. Wang, B. Lyon, A. Kumar, J. Nakamura, and N. Henderson, 2015: Causes of the 2011-14 California drought. J. Climate, 28, 6997-7024, doi: 10.1175/JCLI-D-14-00860.1

Sheffield, J., E.F. Wood, and M.L. Roderick, 2012: Little change in global drought over the past 60 years. *Nature*, **491**, 435–438, 15 November, doi: 10.1038/nature11575.

Svoboda, M., and Coauthors, 2002: The Drought Monitor. *Bull. Amer. Meteor. Soc*., **83**, 1181–1190. doi: 10.1175/1520-0477%282002%29083<1181%3ATDM>2.3.CO%3B2.

Thornthwaite, C.W., 1948: An approach toward a rational classification of climate. *Geogr. Rev.*, **38**, 55–94. doi: 10.2307/210739.

Trouet, V., A.H. Taylor, A.M. Carleton, and C.N. Skinner, 2009: Interannual variations in fire weather, fire extent, and synoptic-scale circulation patterns in northern California and Oregon. *Theor. Appl. Climatol.*, **95(3-4)**, 349–360, doi:10.1007/s00704-008-0012-x.

van der Schrier, G., P.D. Jones, and K.R. Briffa, 2011: The sensitivity of the PDSI to the Thornthwaite and Penman-Monteith parameterizations for potential evapotranspiration. *J. Geophys. Res.*, **116**, doi:10.1029/2010JD015001.

Vicente-Serrano, S.M., J.I. López-Moreno, S. Beguería, J. Lorenzo-Lacruz, C. Azorin-Molina, and E. Morán-Tejeda, 2012: Accurate computation of a streamflow drought index. *J. Hydrol. Eng.*, **17(2)**, 318–332, doi:10.1061/(ASCE)HE.1943-5584.0000433.

Weiss, J.L., C.L. Castro, and J.T. Overpeck, 2009: Distinguishing pronounced droughts in the southwestern United States: Seasonality and effects of warmer temperatures. *J. Climate*, **22**, 5918–5932, doi: 10.1175/2009JCLI2905.1.

680 Xia, Y. and Coauthors, 2012a: Continental-scale water and energy flux analysis and validation
681 for the North American Land Data Assimilation System project phase 2 (NLDAS-2): 1.
682 Intercomparison and application of model products. *J. Geophys. Res.*, **117(D3)**,
683 doi:10.1029/2011JD016048.
684 Xia, Y. and Coauthors, 2012b: Continental-scale water and energy flux analysis and validation
685 for the North American Land Data Assimilation System project phase 2 (NLDAS-2): 2.
686 Validation of model-simulated streamflow, *J. Geophys. Res.*, **117(D3)**,
687 doi:10.1029/2011JD016051.
688 Yao, Y., S. Liang, Q. Qin, and K. Wang, 2010: Monitoring drought over the conterminous
689 United States using MODIS and NCEP Reanalysis-2 data. *J. Appl. Meteor. Climatol*., **49**,
690 1665–1680. doi:10.1175/2010JAMC2328.1.

691 **Table 1:** Drought classes for comparing USDM to SPI, SSI, ESI, and EDDI. Positive EDDI
692 values indicate drought with the upper percentiles (70-100) used to derive USDM classes.
693

USDM drought category	Description	SPI, SSI, and ESI percentiles	EDDI percentiles
D0	Abnormally Dry	21-30	70-79
D1	Moderate Drought	11-20	80-89
D2	Severe Drought	6-10	90-94
D3	Extreme Drought	3-5	95-97
D4	Exceptional Drought	0-2	98-100

694

List of figures:

Figure 1: Correlation coefficients between EDDI and SPI at **(a)** 1-month, **(c)** 6-month, **(e)** 12-month, and SSI **(b)** 1-month, **(d)** 6-month, and **(f)** 12-month timescales. Correlations were computed at each grid point for 1979 to 2013 over each month (n = 35) and then averaged over all months in each timescale.

Figure 2: Case study areas. Shading indicates METDATA terrain height (m) and red boxes indicate area-averaging domains for Figure 3. IA, TX, and PA boxes are 50 x 100 4-km METDATA pixels (200 km x 400 km), and CA box is 25 x 25 pixels (100 km x 100 km). Blue patches indicate area-averaging domains for flash drought cases in Figure 8.

Figure 3: Monthly correlations between EDDI and SPI (top row) and SSI (bottom row) at all timescales for **(a, e)** central TX, **(b, f)** the CA Central Valley, **(c, g)** IA, and **(d, h)** PA. Y-axis indicates ending month of each timescale, and x-axis shows timescale (months). Shading indicates correlation coefficients. Correlations were computed at each grid point for 1979 to 2013 (n = 35) and then averaged over each climate region.

Figure 4: Seasonal (April through September) correlation coefficients (left column spring and right column summer) between ESI and EDDI at **(a, b)** 4-week, **(c, d)** 8-week, and **(e, f)** 12-week timescales. Areas in white indicate an insufficient amount of ESI data. Correlations were computed at each grid point for 2000 to 2013 over each week (n = 14 years) and then averaged over all months.

Figure 5: EDDI under sustained and flash drought conditions. Monthly time series of 1-month EDDI, SSI, and SPI area averaged over the IA domain for 2011 and 2012. Note that the vertical axis of EDDI is inverted to clearly visualize drought onset and duration relative to SPI and SSI. Light green reference line indicates start of moderate drought classification (EDDI = 0.78, SPI and SSI = -0.78).

Figure 6: (a) Monthly time series (values on the last day of each month) of 1-month EDDI and EDDI constrained by climatology T_{air} (EDDI-T), q (EDDI-q), R_d (EDDI-R_d), and U (EDDI-U) for 2011 and 2012. Black box highlights time period shown in (b). **(b)** Daily time series of 1-month EDDI, EDDI-T, EDDI-q, EDDI-R_d and EDDI-U for May and June 2011 shown to highlight details of flash drought initiation. Each day in the time series uses the previous 30-day accumulated E_0. Note that the vertical axis of EDDI is inverted. Light green reference line indicates start of moderate drought classification (EDDI = 0.78).

Figure 7: Evolution of the USDM **(top row)**, 1-month EDDI **(second row)**, 1-month ESI **(third row)**, 1-month SSI **(fourth row)**, and 1-month SPI **(fifth row)** through the spring and summer of 2012. USDM data are from 1 May, 2012 (April column), 5 June, 2012 (May column), 3 July, 2012 (June column), and 31 July, 2012 (July column). EDDI, ESI, SSI, and SPI are at 1-month timescales at the end of each month. All drought metrics have been converted to USDM categories according to **Table 1**.

Figure 8: Flash drought case studies using daily time series of 1-month EDDI (red line), 1-month SPI (blue line), and 1-month SSI (green line). Note that the vertical axis of EDDI is inverted to clearly visualize drought relative to SPI and SSI. Averaging domains are shown as blue patches in **Figure 2** and include PA **(first row)**, NY **(second row)**, WI **(third row)**, and OH-IN **(fourth row)**. Black boxes highlight the periods of flash drought.

Figure 9: Spatial comparison of drought metrics across the western US. **Row 1**: USDM from **(a)** 25 June, 2002, **(b)** 2 October, 2007, **(c)** 31 March, 2015, and **(d)** 1 September, 2015. **Row 2**: **(e)** 6-month EDDI, June, 2002, **(f)** 12-month EDDI, September, 2007, **(g)** 6-month EDDI, March, 2015, and **(h)** 6-month EDDI, August, 2015. **Row 3**: **(i)** 6-month SSI, June, 2002, **(j)** 12-month SSI, September, 2007, **(k)** 6-month SSI, March, 2015, and **(l)** 6-month SSI, August, 2015. **Row 4**: **(m)** 6-month SPI, June, 2002, **(n)** 12-month SPI, September, 2007, **(o)** 6-month SPI, March, 2015, and **(p)** 6-month SPI, August, 2015.

Figure 10: Area-averaged time series of EDDI over the northern Sierra Nevada from 1979 to 2014 aggregated at 2-week (a), 1-month (b), 3-month (c), 6-month (d), and 12-month timescales. Red boxes highlight the four most prominent hydrologic droughts during the time period.

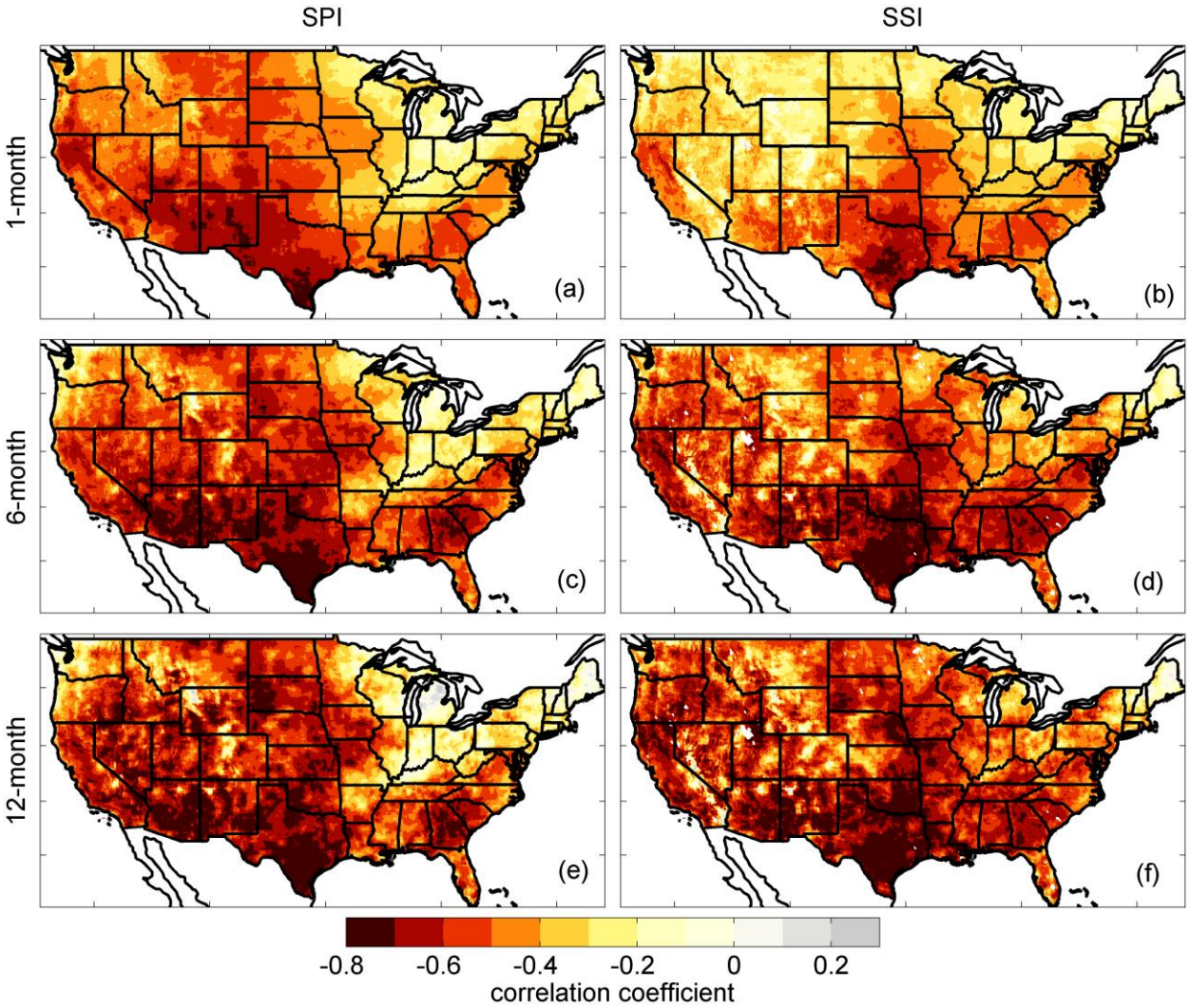

Figure 1: Correlation coefficients between EDDI and SPI at **(a)** 1-month, **(c)** 6-month, **(e)** 12-month, and SSI **(b)** 1-month, **(d)** 6-month, and **(f)** 12-month timescales. Correlations were computed at each grid point for 1979 to 2013 over each month (n = 35) and then averaged over all months in each timescale.

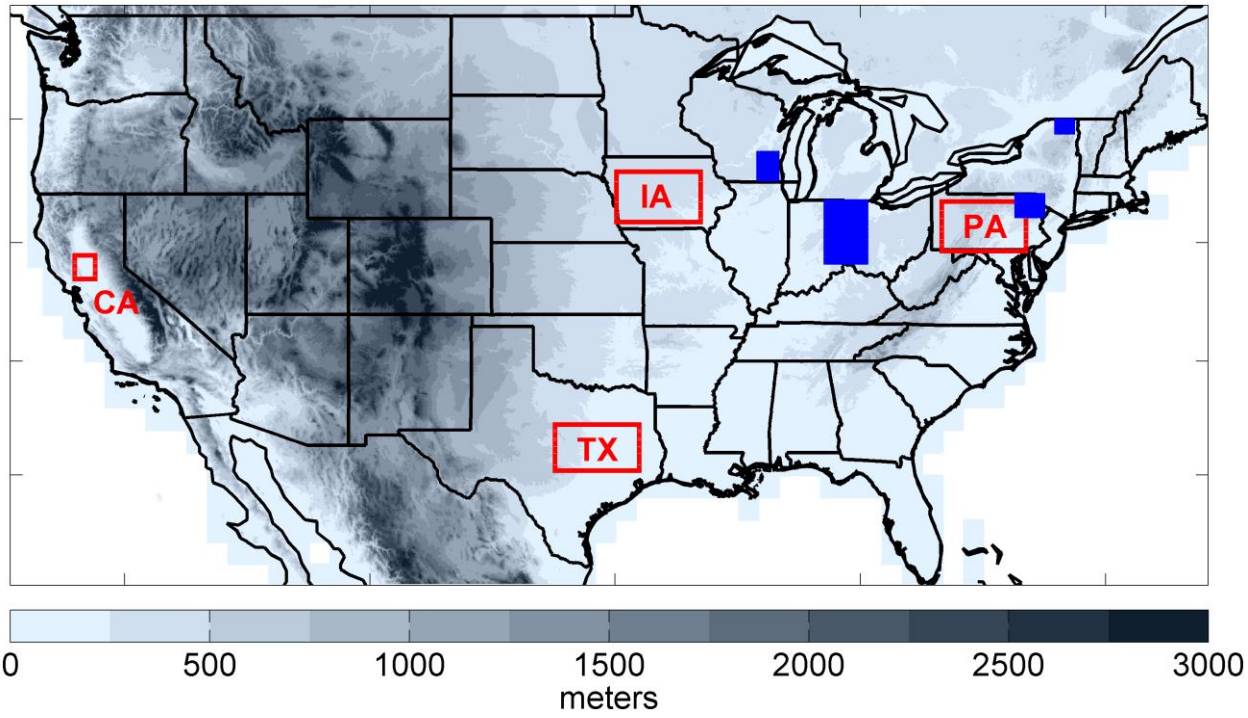

763

764 **Figure 2:** Case study areas. Shading indicates METDATA terrain height (m) and red boxes
765 indicate area-averaging domains for Figure 3. IA, TX, and PA boxes are 50 x 100 4-km
766 METDATA pixels (200 km x 400 km), and CA box is 25 x 25 pixels (100 km x 100 km). Blue
767 patches indicate area-averaging domains for flash drought cases in Figure 8.

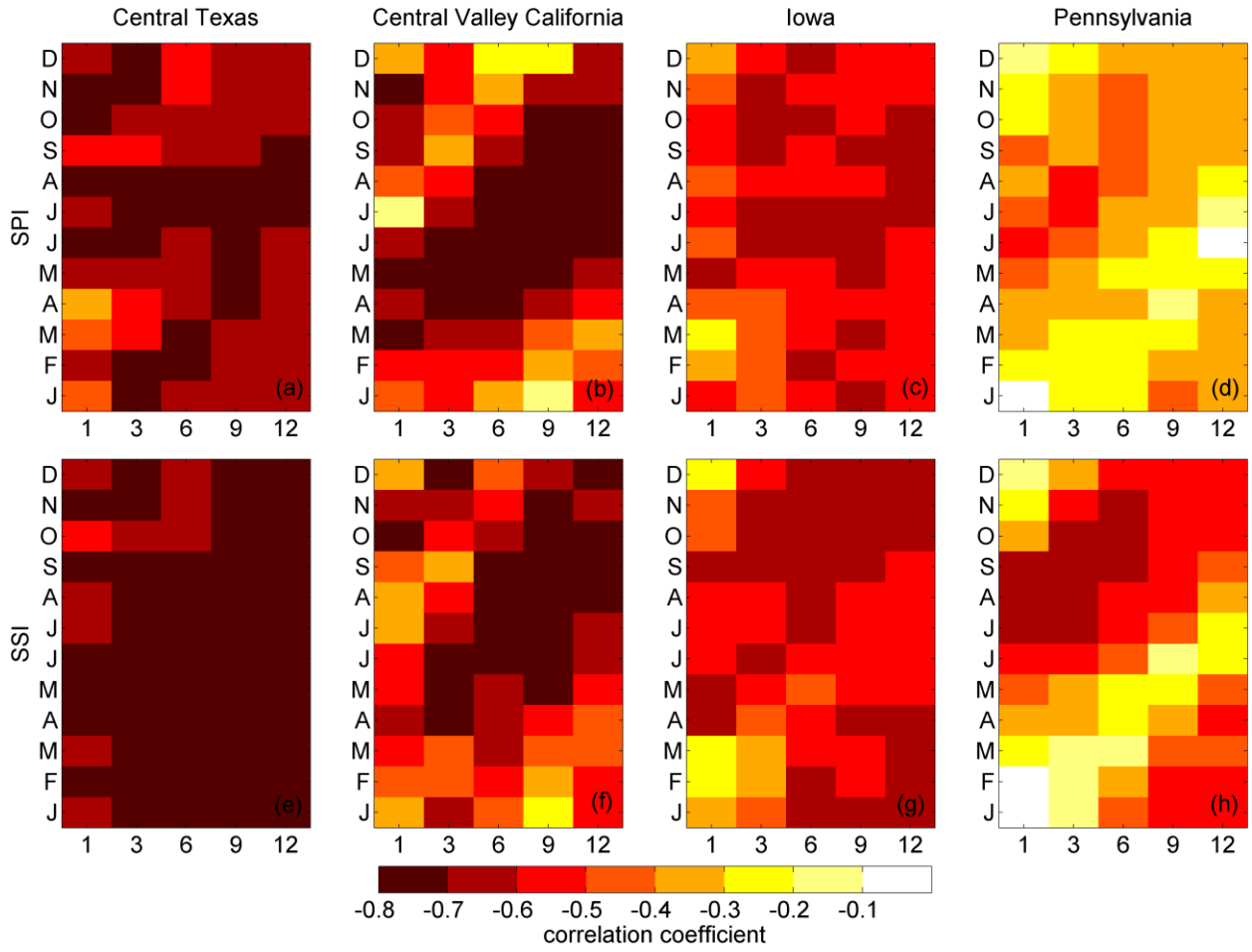

768

769 **Figure 3:** Monthly correlations between EDDI and SPI (top row) and SSI (bottom row) at all
770 timescales for **(a, e)** central TX, **(b, f)** the CA Central Valley, **(c, g)** IA, and **(d, h)** PA. Y-axis
771 indicates ending month of each timescale, and x-axis shows timescale (months). Shading
772 indicates correlation coefficients. Correlations were computed at each grid point for 1979 to
773 2013 (n = 35) and then averaged over each climate region.
774
775

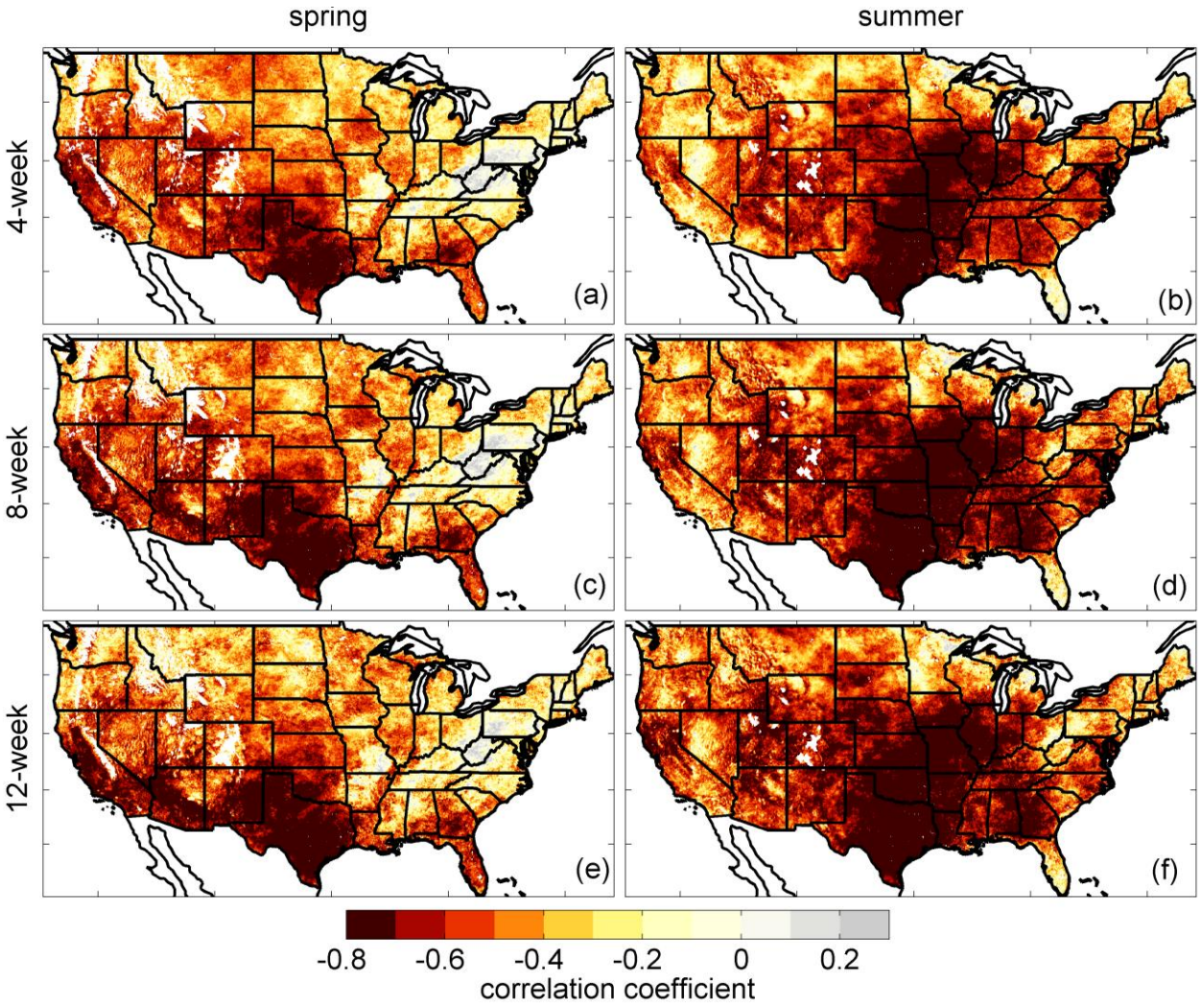

Figure 4: Seasonal (April through September) correlation coefficients (left column spring and right column summer) between ESI and EDDI at **(a, b)** 4-week, **(c, d)** 8-week, and **(e, f)** 12-week timescales. Areas in white indicate an insufficient amount of ESI data. Correlations were computed at each grid point for 2000 to 2013 over each week (n = 14 years) and then averaged over all months.

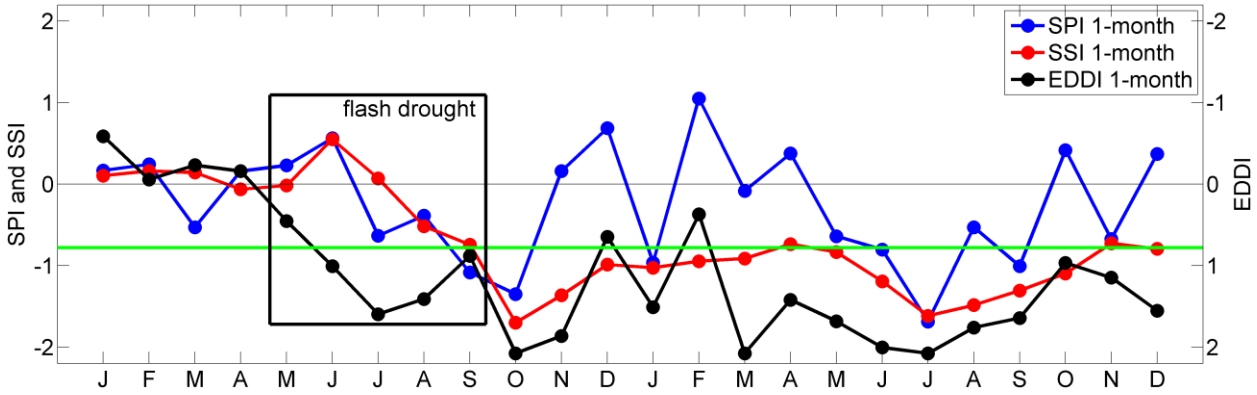

Figure 5: EDDI under sustained and flash drought conditions. Monthly time series of 1-month EDDI, SSI, and SPI area averaged over the IA domain for 2011 and 2012. Note that the vertical axis of EDDI is inverted to clearly visualize drought onset and duration relative to SPI and SSI. Light green reference line indicates start of moderate drought classification (EDDI = 0.78, SPI and SSI = -0.78).

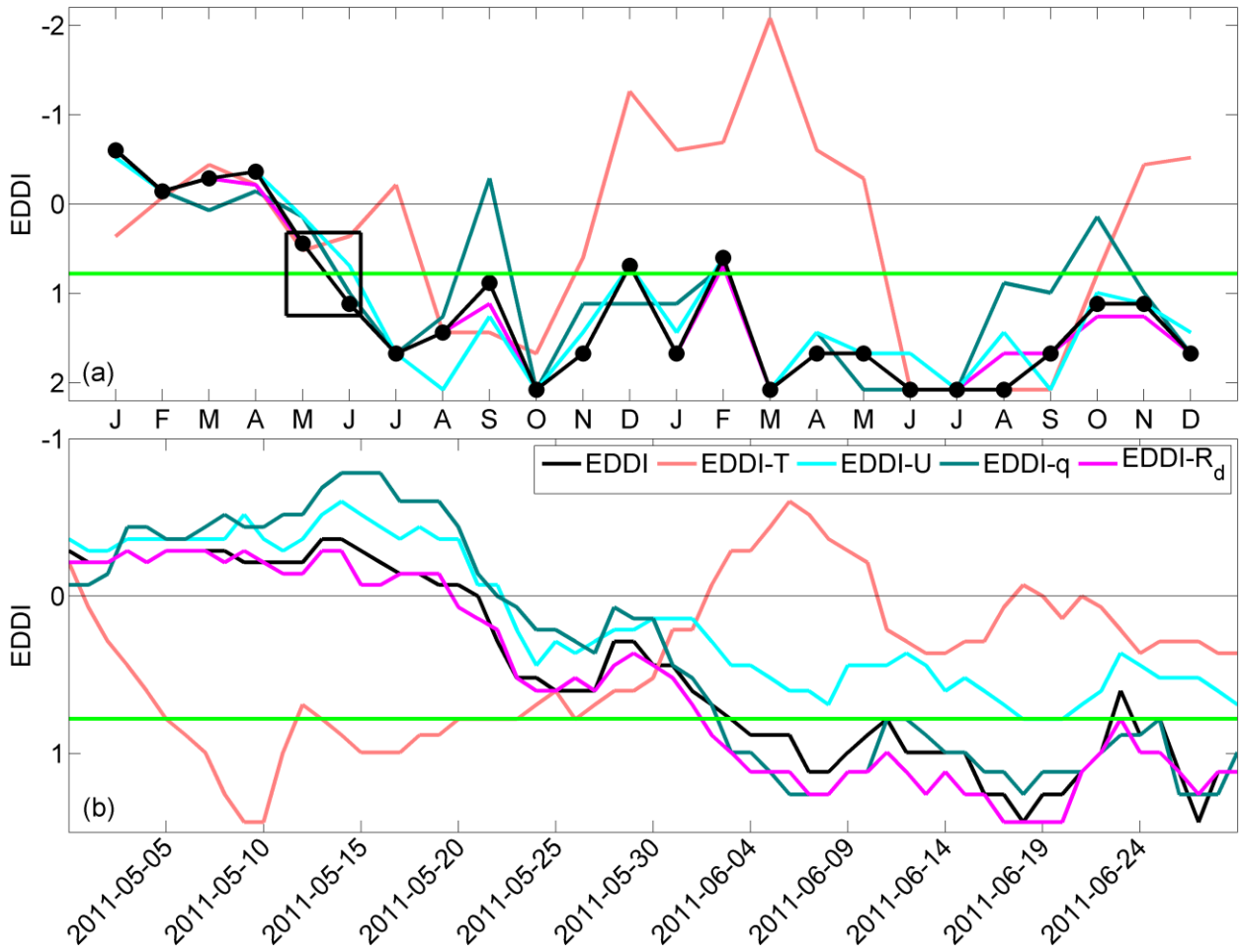

Figure 6: (a) Monthly time series (values on the last day of each month) of 1-month EDDI and EDDI constrained by climatology T_{air} (EDDI-T), *q* (EDDI-q), R_d (EDDI-R_d), and *U* (EDDI-*U*) for 2011 and 2012. Black box highlights time period shown in (b). **(b)** Daily time series of 1-month EDDI, EDDI-T, EDDI-q, EDDI-R_d and EDDI-*U* for May and June 2011 shown to highlight details of flash drought initiation. Each day in the time series uses the previous 30-day accumulated E_0. Note that the vertical axis of EDDI is inverted. Light green reference line indicates start of moderate drought classification (EDDI = 0.78).

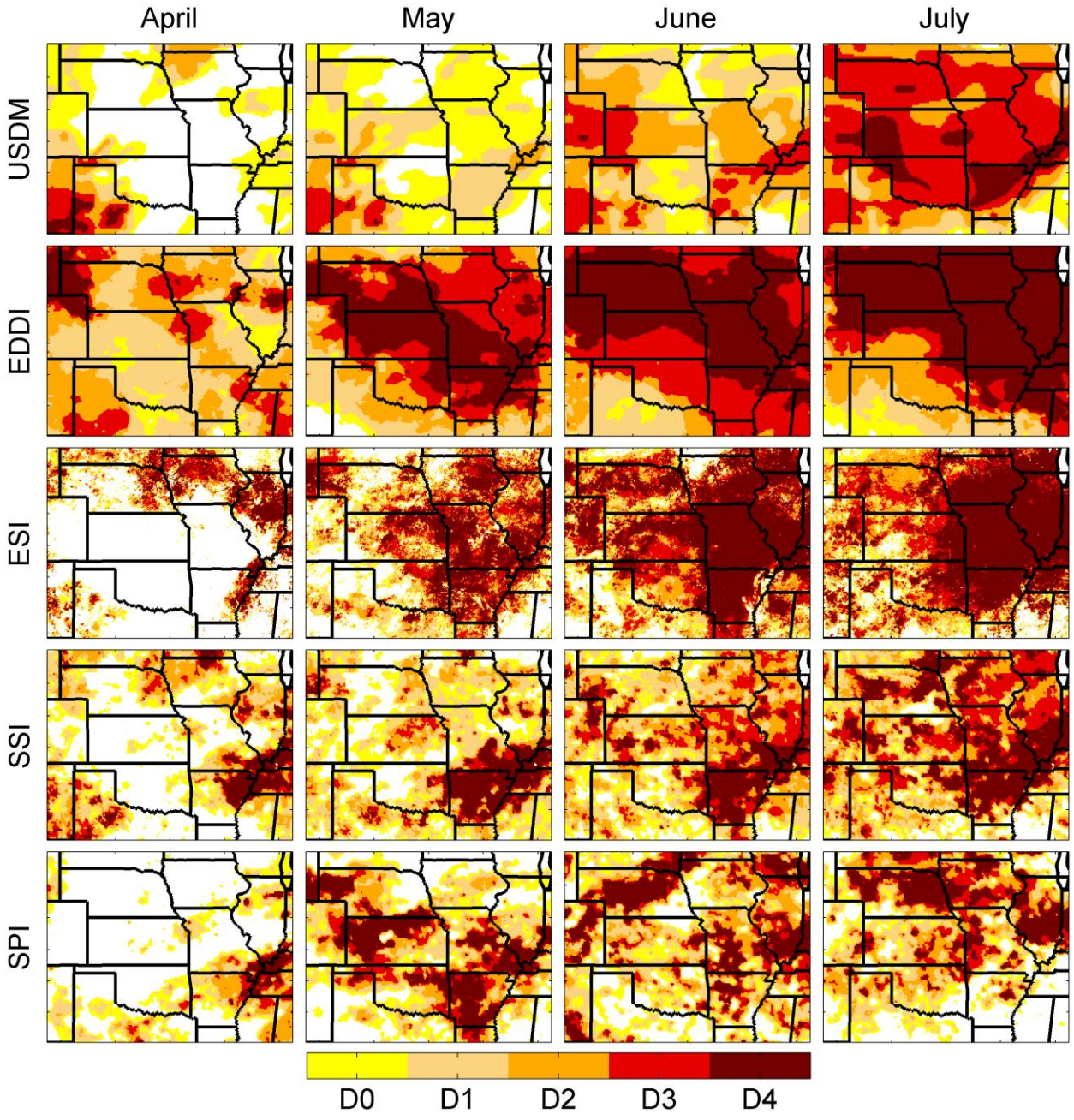

Figure 7: Evolution of the USDM **(top row)**, 1-month EDDI **(second row)**, 1-month ESI **(third row)**, 1-month SSI **(fourth row)**, and 1-month SPI **(fifth row)** through the spring and summer of 2012. USDM data are from 1 May, 2012 (April column), 5 June, 2012 (May column), 3 July, 2012 (June column), and 31 July, 2012 (July column). EDDI, ESI, SSI, and SPI are at 1-month timescales at the end of each month. All drought metrics have been converted to USDM categories according to **Table 1**.

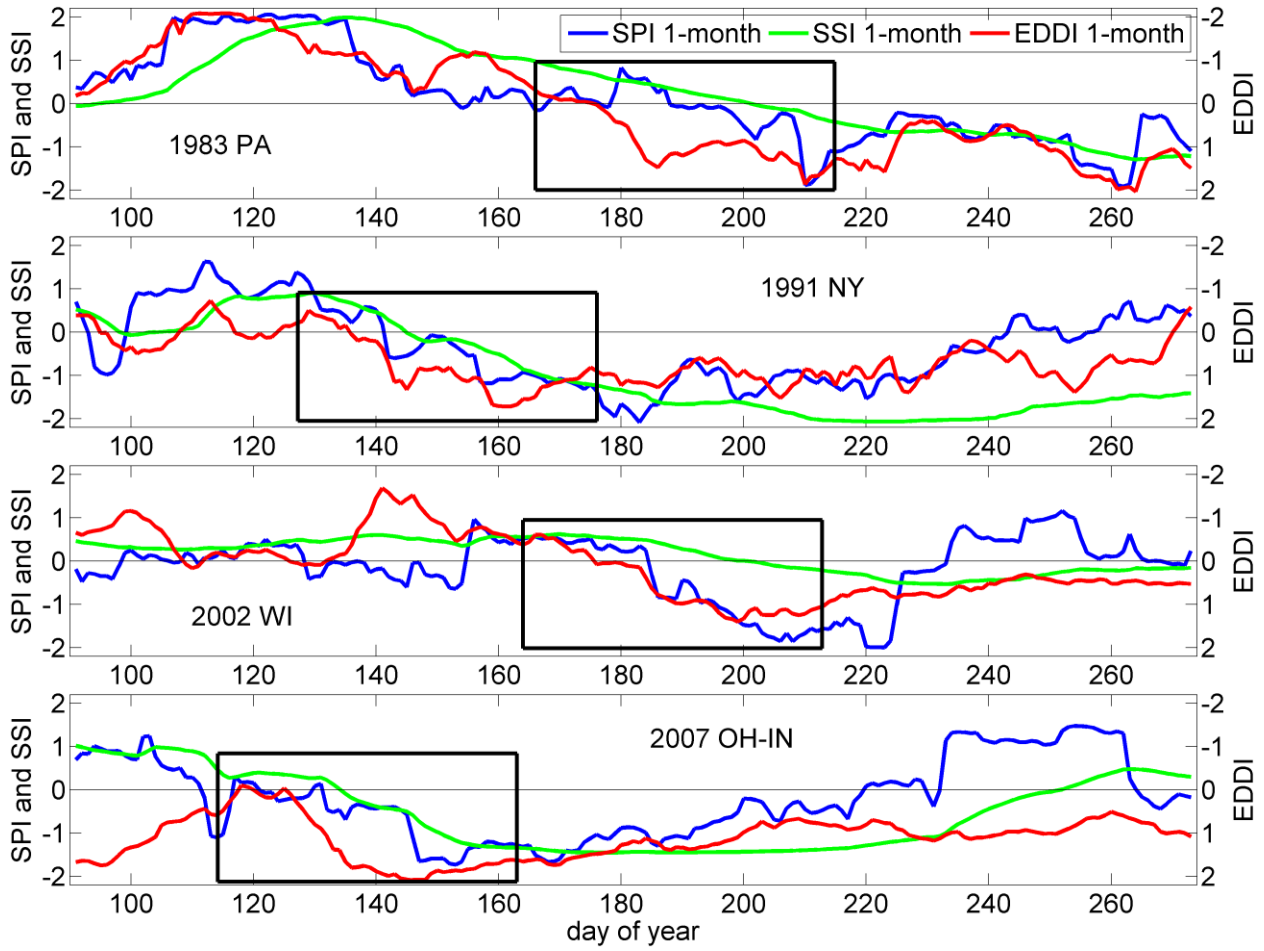

Figure 8: Flash drought case studies using daily time series of 1-month EDDI (red line), 1-month SPI (blue line), and 1-month SSI (green line). Note that the vertical axis of EDDI is inverted to clearly visualize drought relative to SPI and SSI. Averaging domains are shown as blue patches in **Figure 2** and include PA **(first row)**, NY **(second row)**, WI **(third row)**, and OH-IN **(fourth row)**. Black boxes highlight the periods of flash drought.

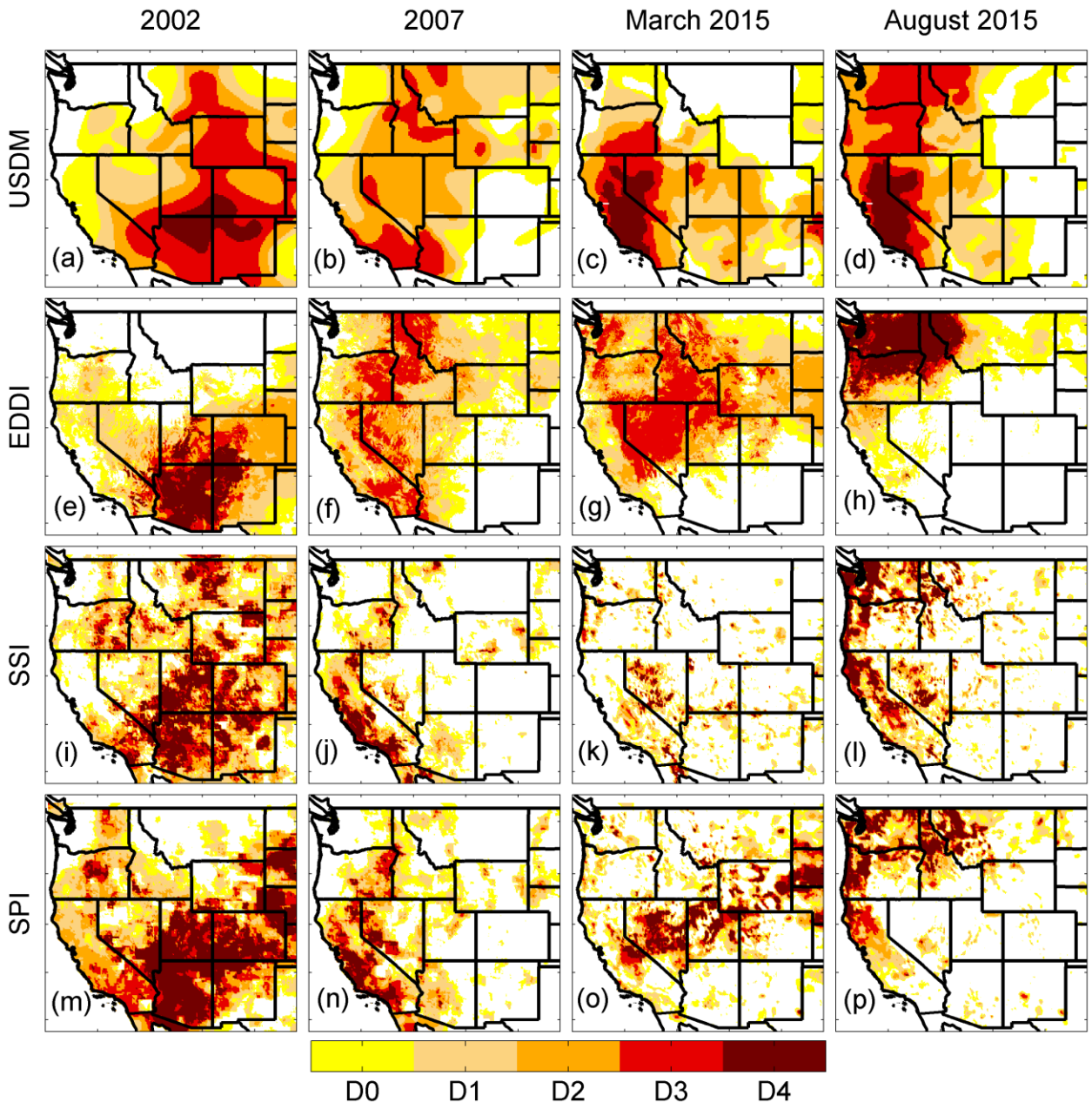

Figure 9: Spatial comparison of drought metrics across the western US. **Row 1**: USDM from **(a)** 25 June, 2002, **(b)** 2 October, 2007, **(c)** 31 March, 2015, and **(d)** 1 September, 2015. **Row 2**: **(e)** 6-month EDDI, June, 2002, **(f)** 12-month EDDI, September, 2007, **(g)** 6-month EDDI, March, 2015, and **(h)** 6-month EDDI, August, 2015. **Row 3**: **(i)** 6-month SSI, June, 2002, **(j)** 12-month SSI, September, 2007, **(k)** 6-month SSI, March, 2015, and **(l)** 6-month SSI, August, 2015. **Row 4**: **(m)** 6-month SPI, June, 2002, **(n)** 12-month SPI, September, 2007, **(o)** 6-month SPI, March, 2015, and **(p)** 6-month SPI, August, 2015.

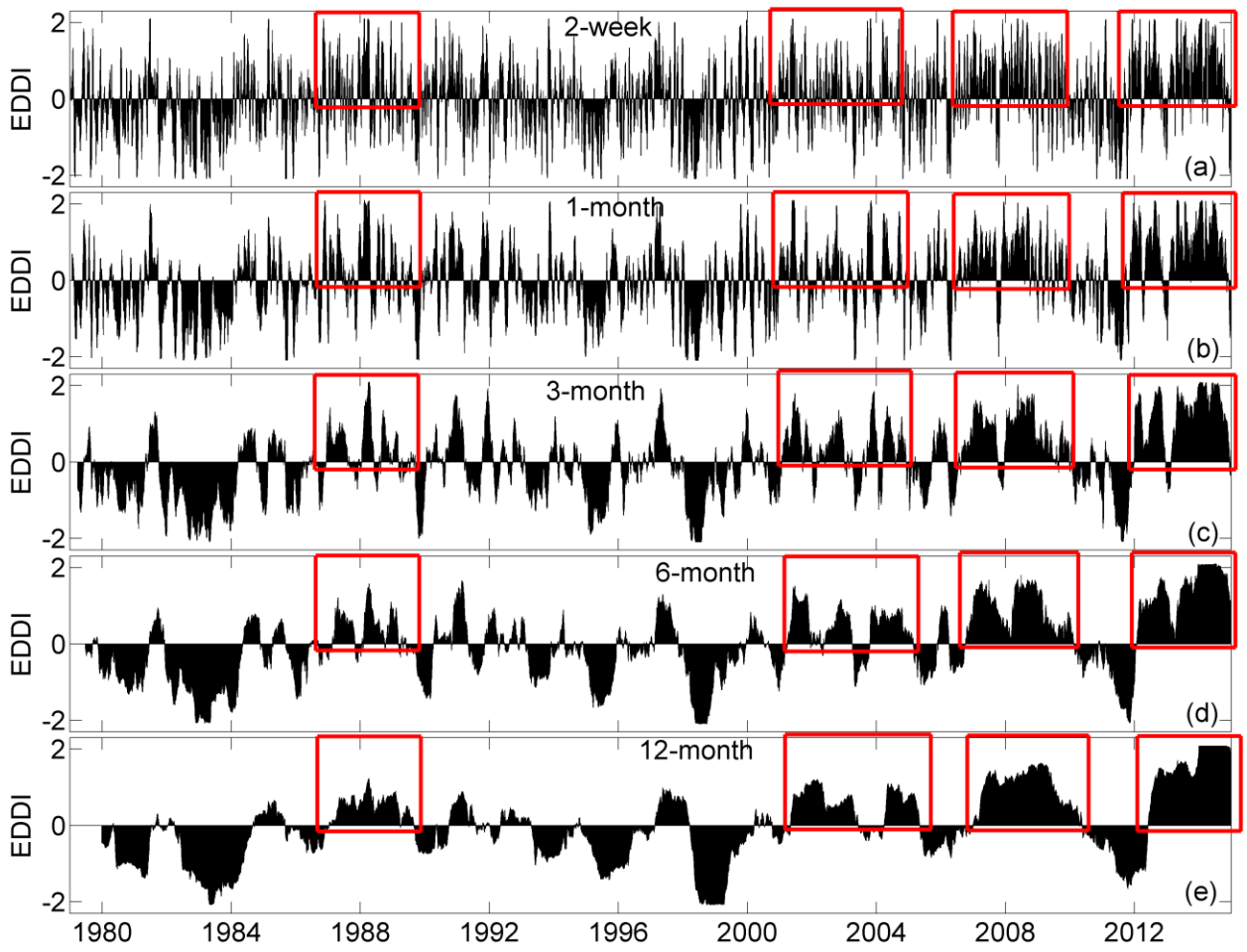

828

829 **Figure 10:** Area-averaged time series of EDDI over the northern Sierra Nevada from 1979 to
830 2014 aggregated at 2-week (a), 1-month (b), 3-month (c), 6-month (d), and 12-month timescales.
831 Red boxes highlight the four most prominent hydrologic droughts during the time period.